Time-dependent behaviour of industrial granular materials under vibration: modelling and phenomenology

Andrea Suaza-Montalvo, Maria Graciela Cares Pacheco, Véronique Falk

Time-dependent behaviour of industrial granular materials under vibration: modelling and phenomenology.

Andrea Suaza-Montalvo[a], Maria Graciela Cares-Pacheco[a,*], Véronique Falk[a]

[a]*Universite de Lorraine, LRGP-CNRS, 1 rue Grandville, Nancy, BP-54001, France*

Abstract

Several industrial and fundamental studies focus on the consolidation of granular materials as this covers many technological fields. When a granular material is shaken, it densifies. The energy needed to compact or decompact a powder column is of great interest in handling, filling and transport operations. This work studies the dynamic behaviour of four industrial granular materials—wheat flour, sericite, microcrystalline cellulose and glass beads—when submitted to vertical vibration using a particle damper. The effect of the vibration wave was studied by varying two dimensionless parameters: the relative acceleration, Γ and relative frequency, Ω including the relaxation time between periods. Our results show that despite the cohesiveness of the samples, their compaction dynamics occurs in at least two-compaction steps that a succession of stretched exponentials can model, denoted herein as a generalised KWW model. Also the absence of a relaxation time between periods leads to fluidisation during the first periods of vibration.

The Fluidisation phenomena–the convective movement, granular jets, bubbling and slugging–appear to enhance particle reorganisation giving rise to higher packing fractions depending on the nature of the grains and operational conditions. A classification of the observed behaviours is proposed and related to the compaction kinetics.

Keywords: Powders, Compaction, Vibration, Fluidisation, Modelling

1. Introduction

Granular materials exist all around us and are used for building, feeding, mining or healing, among other uses [1]. Despite their omnipresence in industry, granular flow is still difficult to describe, measure and predict [2]. Granular materials behave differently from liquids or solids, in particular because their bulk density, ρ, changes under the influence of external mechanical forces such as impact, vibration and compression [3]. Several industrial processes and operations subject materials to vibration, so their behaviour under vibration has been thoroughly studied [4]. When granular materials are vibrated, the bulk can compact [5], dilate [6], segregate by size [7], and even fluidize [8]. Phenomena such as arching, heaping, segregation, surface waves, convection and wave propagation through the bed have been observed [9]. All these phenomena can be used intelligently to ensure process feasibility but they can also generate several problems [6].

The densification of powders under vibration can be associated with the handling, processing and storage conditions involved [10]. In granular mechanics, densification under vibration is used to determine energy dissipation–attenuation [11]. Powders technology groups use densification, or compactness, to describe flowability [12, 13, 14]—the more compressible a material is, the less flowable it will be [15]. We can thus argue that densification is a valuable method for characterizing granular materials that has been widely studied by the soil mechanics community. Still, the fundamental principles that govern densification are not well established. In the case of soft vibration, some insides have been given for cohesionless particles, with the simplest interpretation based on free-volume models [16, 17]. The case of strong vibration—presented herein—is more complex because the grains can behave as a solid, a liquid, or a gas. In this context, there are no fundamental principles describing densification because no constitutive equations are available between the continuous and discrete approaches—at least not to describe industrial granular materials [2].

*Corresponding author

Email address: maria-graciela.cares@univ-lorraine.fr (Maria Graciela Cares-Pacheco)

Densification under vibration

When a powder is gently shaken, it densifies if the energy supplied allows new arrangements opportunities for the grains. Assuming that the grains do not undergo deformation, densification results from the competition between collective grain arrangements—reducing the bulk volume or porosity—and the size exclusion between grains that tends to keep a grain trapped around its neighbours [18]. The densification dynamics is a response of the grains to two variables: the vibration itself [19] and the system geometry [5, 9]. The system geometry is characterised by the relation between the diameter of the container (D) and the grains (d). There are two main ways in terms of motion to vibrate powders namely harmonic and tapping. Harmonic motion is obtained using particle dampers (shaker) excited with a sinusoidal signal [13, 20] while tapping is generated by rotating a snail cam [21], resulting in a shock wave per rotation. In tapping devices, the amplitude is the free-fall height of the system and f is the snail cam rotation rate. In harmonic motion, if we consider a pile of grains under gravity g subjected to a vertical vibration $A \sin \omega t$, where $\omega = 2\pi f$ is the angular frequency of the vibration and so f is the signal frequency, and A the amplitude of the motion. Despite the geometrical configuration (grain size, vessel, the grains' column-height), the vibration is controlled by two dimensionless numbers. The first is the vibrational intensity or relative acceleration $\Gamma = a/g$, relating the imposed acceleration a and the acceleration due to gravity g. The second is the relative frequency $\Omega = \omega/\sqrt{g/d}$ that compares the time it takes to one grain to fall under gravity over a distance equal to its size and the signal period ω [17].

Most of the reported experimental studies allow the system to relax between two consecutive periods by imposing regular intervals of one second [22, 20]. This time t_w is added to ensure that all movement in the column is stopped before the subsequent excitation takes place [13]. The main idea is to avoid oscillations due to the anisotropic velocity of the grains. The system's centre of mass must stay at rest and remain in equilibrium before the following excitation. Furthermore, well-separated signals, or "taps", can avoid internal resonances when working with long tubes.

The vibration amplitude appears to be the parameter that defines what type of phenomena will be observed [1]. However the relationship between kinetic and potential energies is also important when waves are present on the surface of the bed [23]. Low-amplitude vibrations induce sound propagation. An increase in the vibration amplitude will produce slow relaxation and changes in the global shape of the granular bed. High amplitude vibrations will produce convection rolls, jets of particles and bubbling [8, 23].

Some authors consider that the fluid-like behaviour starts because of the lift-off of the granular material from the bottom of the container during the vibration cycle. It is presented as "slightly more than one" Γ [23] and for monodisperse glass beads (1 mm $< d <$ 4 mm), and sand ($250\ \mu$m $< d <\ 600\mu$m) it corresponds to the same non-dimensional acceleration for all frequencies ($\Gamma = 1.2$) [8]. As a shear threshold, it is related to the internal friction of the material but as this was essentially determined for free-flowing materials, the cohesive forces that are important for powders used industrially have not been considered.

Densification dynamics - Modelling

The compaction dynamic considers the evolution of the volume of the pile V_{total} as a function of the number of vibrations N (taps or sinusoidal periods). The evolution of $V(N)$ is expressed using a dimensionless number, the packing fraction ϕ (Eq. 1). It relates the volume of the particles V_p to V_{total} and quantifies the space available for the particles to reorganize themselves within the bulk:

$$\phi = \frac{V_p}{V_{total}} = \frac{m}{\rho_p \cdot V_{total}} = \frac{\rho}{\rho_p} \tag{1}$$

where ρ_p is the envelope density of the particles (equal to the pycnometric density for non-porous particles) and m is the mass of the material.

The relation $\phi(N)$ for dry granular materials has been empirically described using different expressions, summarised in the following paragraphs and table 1. It could be argued that powder technology groups have mostly studied industrial-sector-related powders under tapping (free fall) while the physics community focused on glass beads in particle dampers (sine wave). Furthermore, the relation D/d used in almost all the studies (94% in table 1) is bigger than 50 to avoid the effect of the walls during densification. The studied frequencies range from 1 to 100 Hz and the vibration amplitude from 0.02 to 250 mm (Table 1).

The first kinetic models were proposed by Kawakita's group [32]. The first is named KKH herein and is also known as Kawakita and Kuno's or Heckel's model (eq. 2). It describes an exponential relation and has been used to describe the compaction of tapped food powders [33, 24].

$$\phi = \phi_\infty - (\phi_\infty - \phi_0)\ \exp -\left(\frac{N}{\tau}\right) \tag{2}$$

Table 1: Summary of the experimental works that study granular compaction

Granular material	D/d	Used model(s)	Vibration type	A [mm]	f [Hz]	t_w
Coffee, flours [24]	NR	Kawakita, Heckel	Tapping	30-250	6.7	Yes
Glass beads, magnesium stearate, talc [25]	3500-14000	NR	Harmonic	NR	20-90	No
Alumina, silicon carbide [26]	NR	KWW, Kawakita, Heckel	Tapping	NR	NR	Yes
Glass beads [22]	9.4	Chicago	Harmonic	0.7-2	30	Yes
Glass beads [27]	19	Chicago	Harmonic	NR	NR	Yes
Glass beads [9]	100	NR	Harmonic	NR	30	Yes
Metallic beads[1] [28]	25	Chicago	Tapping	NR	2	Yes
Glass beads [20]	100	KWW	Harmonic	NR	30, 60, 90	NR
Ballast [29]	30-80	Chicago	Harmonic	0.7-1.3	3.3-6	No
Glass or zirconium beads[2] [30]	37-200	Chicago, KWW	Harmonic	0.02-0.2	30-80	No
Kaolin, MCC, $CaHPO_4$, sand [18]	30-3700	Chicago generalization	Tapping	3	4.17	Yes
Glass beads, alumina, UO_2 [31]	100, 500	Double KWW	Harmonic[3]	NR	30-100	NR
Lactose, MCC, food powders [13]	100-2500	KWW	Tapping	NR	1, 4.17	Yes
Glass beads, sand, food powder, biomass, seeds [19]	NR	KWW	Tapping	3-16	2.5-5	Yes
Avicel® PH102, Retalac® [14]	110-200	KWW, Chicago	Tapping	3	4.17	Yes

MCC: microcrystalline cellulose, NR: Not reported, [1]2D study, [2]fluid saturated granular suspension, [3]Horizontal

where the subindex 0 and ∞ correspond to the packing fraction at the time 0 and the end of the experience, mostly when no evolution is observed, and τ is a characteristic relaxation time representing the arrangement of grains until the final steady-state.

The second was inspired by their uniaxial compression model, which states: "Compressibility is proportional to the porosity of the material" [34]. This model has successfully described the dynamic of compaction under tapping for food powders [33, 24], alumina and silicon carbide powders [26] and microcrystalline cellulose [18].

$$\phi = \frac{\phi_0(1 + BN)}{1 + BN(1 - A)} \tag{3}$$

where A and B are constants regressed from experimental data. A has been associated with intergranular friction, cohesion and the Hausner ratio [33] while B to compressibility [18]; still, for the same material, very different behaviours can be observed depending on the energy supplied to the system. Thus, A and B have no clear physical interpretation and remain correlation-based [18, 32, 33].

The Kohlrausch-Williams-Watts model (KWW) is a modification of the KKH model (Eq. 4) and started to be used around 1994 to describe the compaction of granular materials [26]. Despite having no clear physical meaning, it has been largely used to describe densification kinetics [13, 14, 20, 26, 9, 30, 18, 31, 19].

$$\phi = \phi_\infty - (\phi_\infty - \phi_0)\, e^{-\left(\frac{N}{\tau}\right)^\beta} \tag{4}$$

where τ is a characteristic time quantifying the compaction dynamics, and β is an adjustment parameter. This model fits a wide range of accelerations showing an Arrhenius-like dependency on Γ-playing the role of a granular temperature [9, 18]. Philippe and Bideau also suggested the existence of an intensity threshold (liftoff threshold) acting as a "potential barrier" regarding the granular mobility in compact systems [9].

Chicago's group [22] proposed a kinetic model explained by a non-thermal analysis using glass beads as non-cohesive 'model samples'. The main difference with the previously cited models is that the bulk density does not decay to a steady state as a single exponential curve but exhibits a logarithmic evolution (Eq. 5). The density plots depended on the taps' amplitude and the packing fraction decreases as depth increases. The Chicago model is the most famous in densification studies under harmonic vibration [14, 28, 29, 30, 18, 35].

$$\phi = \phi_\infty - \frac{(\phi_\infty - \phi_0)}{1 + Cln(1 + \frac{N}{\tau})} \tag{5}$$

where C is a fitting parameter, τ is a relaxation time that depends only on the relative acceleration, Γ. Boutreaux and de Gennes gave the theoretical explanation of the model based on free volume and geometrical exclusion at the grain scale [16].

To summarize, except for the Chicago model, all these models correlate experimental results involving adjustment parameters that are not based on local physics. The differences between exponential and logarithmic models can be associated with wall effects due to the geometrical configuration–grain size, vessel and the grains' column-height. The logarithmic model is used to describe configurations with strong boundary effects, such as the Chicago group ($D/d = 9.4$), in which particles move convectively along the tube [36, 22]. While exponential models, such as the one developed by the Rennes group ($D/d = 100$), appear to describe better low confinement configurations [37, 38, 39, 20].

It is commonly accepted that the dynamic of compaction $\phi(N)$ can be described as a logarithmically slow process that occurs in two phases– rapid and slow–until an asymptotical packing fraction ϕ_∞ is achieved [18]. It should be noted that most of these studies are evaluated under "gentle" shaking [20]. When more intense vibrations are applied, the behaviour becomes even more complex and several compaction steps can be observed [31]. Recent propositions describe this type of densification dynamics through a stochastic model [31] announced to be representative of cohesive samples showing a double stretched exponential function as an extended KWW model. Most theoretical approaches are based on free volume arguments (free volume model [16], tetris-like model [40] and parking model [41]), or statistical mechanics approaches relating granular densification with thermal glassy systems—a thermodynamical description of granular media [38]. Despite this, no rheological laws exist for powders (other than glass beads and sand) that predict densification kinetics, and their industrial manipulations are still based on empirical observations.

All these elements bring to the fore the dependence between the vibration conditions, the powders and the phenomenology. It is currently still unclear how to predict densification and how it can be related to processing conditions. A combined analysis of the conditions at which different phenomena occur during densification could be the key to understanding their behaviour and connecting it to processing conditions. Herein, we aim to model the dynamic behaviour of powders under vibration. We will describe and analyse granular compaction as a function of the dimensionless

variables Γ and Ω considering, or not, the relaxation between periods, t_w. We will mainly focus on the phenomena observed and relate them to the densification curves and the final packing fraction.

2. Materials and methods

2.1. Powder samples

Four different granular materials were chosen based on their flow behaviour. Two had good flowability - glass beads and Avicel® PH102 from Dupont - and two had poor flow behaviour - wheat flour from the J. Pousignon mill, located in Fouligny, France and sericite, provided by a cosmetics company. The samples were conditioned under strict air humidity conditions at 20% RH as described in previous work [14] and their water activity, A_w, was quantified.

2.2. Physical characterisation

The powders' size distributions were characterised by laser diffraction using a Mastersizer 3000 from Malvern Panalytical. All powders were measured in triplicate using absolute ethanol as the dispersant. The density of the particles was determined from true density measurements (non-porous samples) using a Helium pycnometer, Accupyc 1330 from micromeritics. At least 7 mL of each powder were placed in the 10 mL capsule and measured in triplicate at 20 °C.

Scanning Electronic Microscopy (SEM) was used to analyse the morphology of the individual particles using a JSM T330A SEM from JEOL, with a field emission gun operating at 5 kV. Before analysis, powders were placed on double-sided tape and metallised with a Gold–Palladium mixture for 6 min using an Ion SPUTTER JFC-1100 under air purge.

A few flow parameters are also presented in order to classify or distinguish behaviours between samples. The flow factor ff and the bulk cohesion c were determined from plastic failure tests using the FT4 powder rheometer from Freeman Technology where the preconsolidation stress was set to 6 kPa [2, 42]. The Hausner ratio was determined using the Densitap® [13, 14]. As fluidisation was a regularly observed phenomenon, the minimum fluidisation velocities v_{mf} were calculated from Grace correlation [43] using the particle's density and Sauter diameter. It should be noted that no other correlation dedicated to the Geldart C group particles has been found.

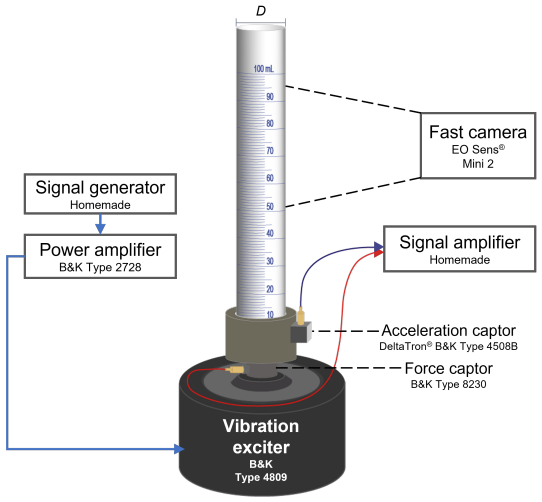

Figure 1: Schema of the experimental device, a homemade particle damper.

2.3. Experimental setup: particle damper

To study the kinetics of compaction, we used a homemade particle damper (Fig. 1) composed by an electromagnetic shaker (vibration exciter type 4809 from B&K) connected to a cylindrical borosilicate glass vessel (D = 26 mm and 240 mm height). The excitation system is made up of a signal generator (homemade) and a power amplifier (type 2718 from B&K). The dynamic of the system is experimentally obtained by an accelerometer glued to the bottom of the vessel - DeltaTron® accelerometer (type 4508B from B&K). Thus, the amplitude of the motion A can be determined from the acceleration a as $A = a/(2\pi f)^2$. Force is measured using a force transducer (type 8230 from B&K) which is screwed into the bottom of the container. The excitation and data acquisition system are controlled using LabVIEW while a fast camera (EO Sens® mini 2 by MotionBLITZ) is used to determine the evolution $\phi(N)$.

The methodology entails using a funnel to pour a fixed amount of powder into the vessel ($V_0 > 45$ mL, 30 g for Avicel® PH102, wheat flour and sericite, and 80 g for glass beads). Special attention is given to start the experiments with a reproducible volume [13]. The high reproducibility of this aerated state during experimental work seems to be related to sample conditioning.

The amplitude of force and acceleration signals corresponds to the peak-to-peak value of the smoothed signals.

To determine the experimental error, five replicates were made for each material. The experimental conditions were selected based on experience according

to the values of Γ and Ω where the greatest variability was observed. As bigger volume reduction is observed during the first steps of compaction only the initial 10 000 periods were analysed in all cases. The total error E_T was determined considering the instrumental E_I and random errors E_R:

$$E_T = \sqrt{E_I^2 + E_R^2} \tag{6}$$

$$E_I = \frac{\rho}{\rho_p}\sqrt{\left(\frac{\Delta\rho}{\rho_p}\right)^2 + \left(\frac{\Delta\rho_p}{\rho_p}\right)^2} \tag{7}$$

$$E_R = \sqrt{\frac{1}{n-1}\sum_{k=1}^{n}(\phi_k - \overline{\phi})^2} \;\; with \;\; \overline{\phi} = \frac{1}{n}\sum_{k=1}^{n}\phi_k \tag{8}$$

where n is the number of repetitions—at least five—and Δ represents the sensitivity of the instrument. It should be noted that the ϕ-error values were always N-related.

For glass beads, the total error on ϕ corresponds to 1.6%, for Avicel® PH102 to 2.0%, for wheat flour to 2.4% and for sericite to 4.6%. For clarity, error bars will not be shown in the graphs and will be assumed to be less than 5%. This worst-case scenario error estimation is based on the long experimental times: data acquisition (over nine hours to reach one million periods for a frequency of 30 Hz) and analysis (frame-by-frame methodology).

3. Results and discussion

3.1. Physical characterisation

Table 2 and figure 2 present the results of the particle analysis of the materials and some data about their bulk behaviour. Sericite is the smallest and widest distributed powder presenting a lamellar shape. Glass beads are next in size, with the narrowest distribution. Avicel® PH102 and wheat flour have similar distribution width and size. Avicel® PH102 have a rod cuboid shape while wheat flour has a rounded irregular shape.

From Geldart's classification, sericite is a cohesive powder, wheat flour is in the transition between cohesive and aeratable powders, Avicel® PH102 and glass beads are aeratable powders. Flowability analysis classifies the samples as:

- Flow factor *ff* classification: glass beads and Avicel® PH 102 flow freely, while sericite and wheat flour are cohesive.

- Hausner ratio classification: glass beads flow freely, wheat flour has passable flow, Avicel® PH102 flow poorly and sericite is very cohesive.

- Observation: in order of increasing flowability, it is the sericite, followed by the wheat flour, the Avicel® PH102 and finally, the best flow corresponds to that of glass beads.

- Minimum fluidisation velocity, v_{mf}, from Grace correlation, in increasing order: sericite, wheat flour, Avicel® PH102 and glass bead. These results are the most dissimilar, which probably is because they do not consider particle cohesion.

3.2. Relaxation time

As shown in table 1, most compaction experiments allow the system to relax between two consecutive periods by imposing regular intervals of t_w = 1 s, or they are carried out with tapping devices [5, 13, 14, 20, 24, 26, 27, 9, 28, 18, 19, 22]. When the system is not allowed to relax—continuous vibration (t_w = 0 ms)—there are no stable configurations between periods and several phenomena occur before reaching a jammed state. For complex granular materials, such as the ones used in this work, the addition of a relaxation time t_w = 300 ms reduces the final packing fraction ϕ_∞ (Fig. 3). Adding time between periods seems to reduce the reorganisation probability, allowing the system to stabilize after each period. Furthermore, most phenomena observed during continuous vibration are not detected when the system is allowed to relax, except convection at the later stages of compaction [44].

allowing the media to relax by adding a time between two periods reduces the final packing fraction

In the following, we will focus on the phenomena occurring during compaction when no relaxation is allowed (no time between periods, t_w = 0 ms). It should be noted that each density plot is composed only of data points where the powder bed's volume could be clearly determined (frame-by-frame analysis).

3.3. Which kinetic model for complex granular materials

Each model presented was fitted to five experimental data sets, representing the main kinetic behaviour of all our data (Fig. 4). Kawakita, KKH, Chicago and KWW models fit one-step compaction kinetics (filled diamonds and empty circles in figure 4) but they lose validity for two-step compaction kinetics, especially when both steps are well separated (filled triangles in figure 4). In these cases, the models represent the initial or final conditions well but not the intermediary states. For two-step compaction kinetics (Fig. 4.E) the use of a double stretched exponential as in the KWW model fits the data appropriately:

$$\phi = \phi_\infty - (\phi_p - \phi_0)\, e^{-\left(\frac{N}{\tau_1}\right)^{\beta_1}} - (\phi_\infty - \phi_p)\, e^{-\left(\frac{N}{\tau_2}\right)^{\beta_2}} \tag{9}$$

Table 2: Granular materials physical characteristics

Granular material	Diameter ±1 [μm] d_{50}	$d_{4:3}$	$d_{3:2}$	$\rho_p \pm 5$ [kg/m^3]	Geldart type	HR	Flowability indicators ff [-] — c [kPa]	v_{mf} [mm/s]
Glass beads	34	36	33	2486	A	1.10	9 - 0.3	1.14
Avicel® PH102	111	122	68	1460	A	1.41	12 - 0.2	2.84
Wheat flour	83	90	25	1570	A-C	1.29	4 - 0.8	0.41
Sericite	9	18	7	2810	C	1.74	3 - 0.9	0.06

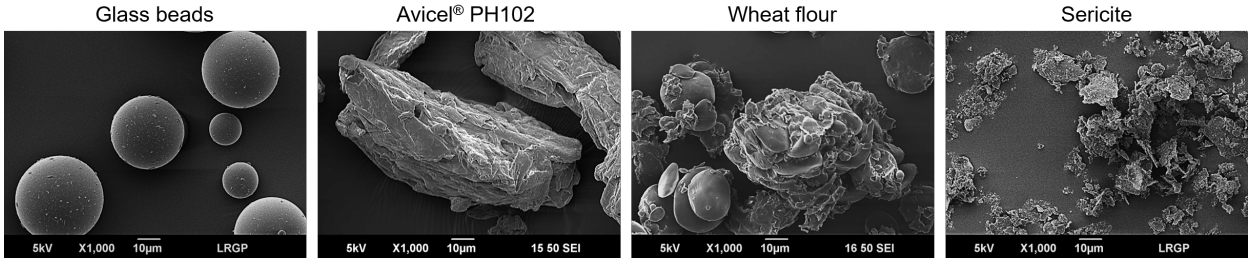

Figure 2: SEM micrographs of granular materials presented in order of increasing surface anisotropy and cohesiveness.

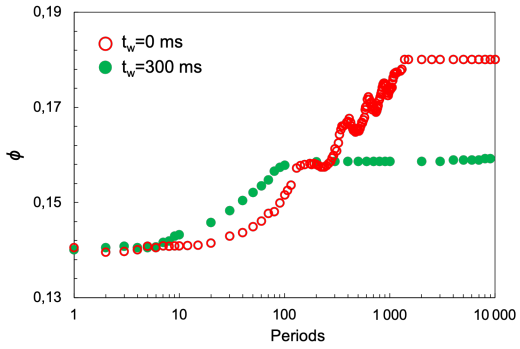

Figure 3: Evolution of the packing fraction of sericite (•) with and (○) without a waiting time between periods at $\Omega = 0.15$ ($f = 30$ Hz) and $\Gamma = 2.5 \pm 0.1$.

with two time-scales τ_1 and τ_2, two exponents β_1 and β_2 and ϕ_p the plateau packing fraction.

The KWW model is relevant when there is one compaction step, while the double KWW model is suitable when there are two. In figure 4, we have shown only one- and two-step compactions but, some experiments result in three-step compactions. When considering the notion of compactions with more than one step, we opted to apply as many stretched exponential functions as necessary to produce the best possible fit for the data. We named this a generalised KWW model. When comparing experimental packing fractions to those determined by the models, the model variation for the four granular materials is always less than 5% (Fig. 5).

Some authors have reported the compaction in more than one step [31, 22, 45] and used two equations to model the experimental data. Mathonnet et al. [31] proposed a physical meaning of the model constants for the kinetics of two-step compaction from a stochastic analysis based on cohesive grains. For these authors, the first compaction step corresponds to a collective reorganisation in clusters and the second to the motion of individual grains. In both steps, the authors define characteristic times (τ) that depend on the number of structures and the initial packing state. Although a succession of stretched exponential functions represents our data well, the proposed physical meaning of the variables [31] is quite far from being validated with our data (the fitting parameter is many orders of magnitude larger). Moreover, the number of "steps" is not related to the cohesiveness of the powders but rather to the vibration parameters (see Fig. 3). The physical meaning of the model variables remains to be found.

3.4. The relative acceleration, Γ

As described in previous works [13], at a given frequency, the final packing fraction (ϕ_∞) can be schematised as shown in figure 6B and described as follows: A first region where the powder bed volume densifies as the vibration amplitude increases. A second region where a maximal compaction state is reached and no evolution of the powder bed volume is observed

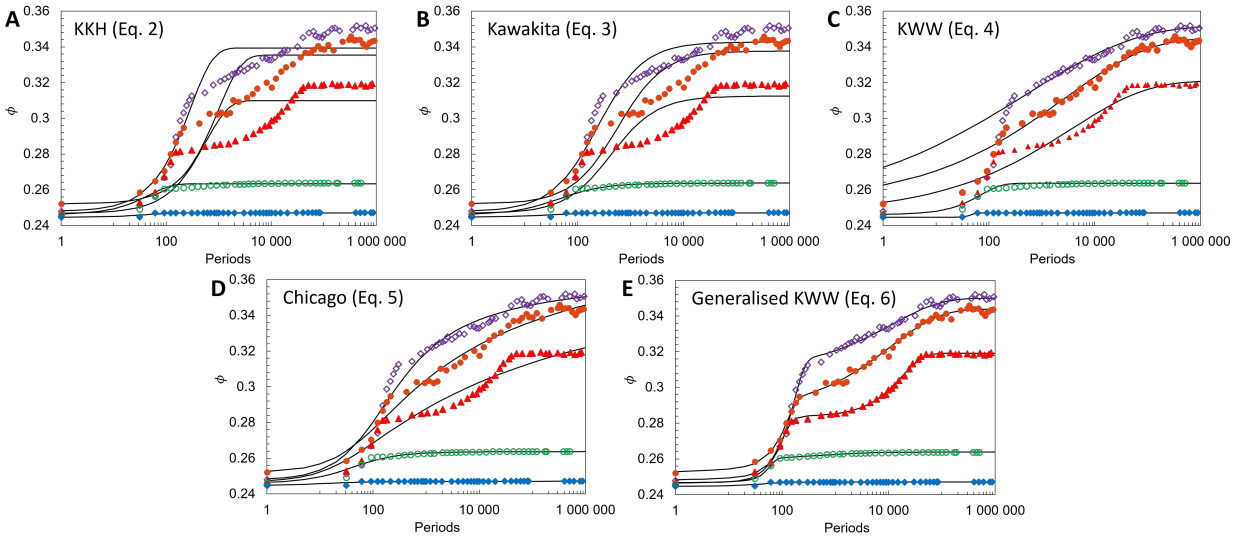

Figure 4: Comparison of compaction models fitting to the different curve behaviours observed for Avicel® PH102 at $\Omega = 0.67$ ($f = 30$ Hz) and ◊ $\Gamma = 8.64$; • $\Gamma = 6.40$; ▲ $\Gamma = 4.00$; ○ $\Gamma = 2.40$; ♦ $\Gamma = 1.33$.

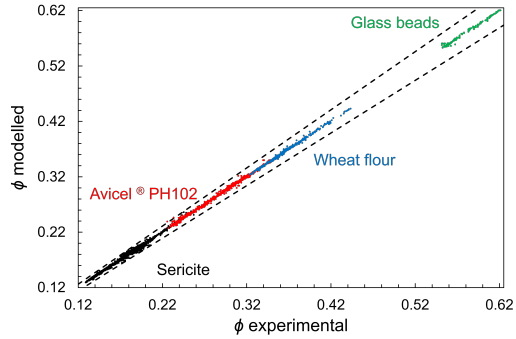

Figure 5: Comparison between experimental and modelled data for the kinetic behaviour of the four granular materials. Dashed lines correspond to a deviation of 5%. Data were modelled by Eq. 9, generalised KWW model, depending on its behaviour.

when increasing Γ. The maximal state of compaction obtained during vibration has been described as an 'ultimate' state, and represents the random close packing experimental limit [13]. Similarly, the maximal packing fraction is denoted herein as the 'ultimate packing fraction', ϕ_U. It should be noted that this region is almost nonexistent for powders that flow well. A third region is observed in which the bulk presents a continuous convective movement that eventually generates the auto-aspiration of air into the powder bed, inducing decompaction.

In the following, we will classify the dynamic behaviour of our four samples into four groups according to the phenomena observed and the shape of the kinetic curves. Three of them occur during the compaction region (Fig. 6A) and the last one during the decompaction region (Fig. 6C).

3.4.1. Solid-like behaviour: one-step compaction

In type I, the granular material behaves as a solid under compression and the densification occurs in a block, as shown in figure 7. We observed this behaviour for all the samples using accelerations close to gravity (Fig. 6A).

When the excitation is not strong enough to allow the particles to jump and separate from each other, bulk densification occurs from the rotation and slip-off of particles by filling the available voids within the granular bed—contact regime. The bulk reorganises through local changes while behaving macroscopically as a solid. The acceleration needed to allow the grains to jump and separate from each other has been previously described as $\Gamma \approx 1.2$ [9, 8]. Our results show that this limit depends on the powder's intrinsic properties and its value increases for poor-flow powders. This is mainly related to the grains' cohesion but not exclusively. For example, for wheat flour $\Gamma > 3.2$ (Fig. 17) while for sericite, $\Gamma > 1.5$. The dissipative nature of granular materials and the nonlinear nature of the contact dynamics could explain this. The energy dissipation of granular systems depends on the material's mechanical properties, such as elasticity and stiffness; more dissipative materials will need higher energies for particles to liftoff.

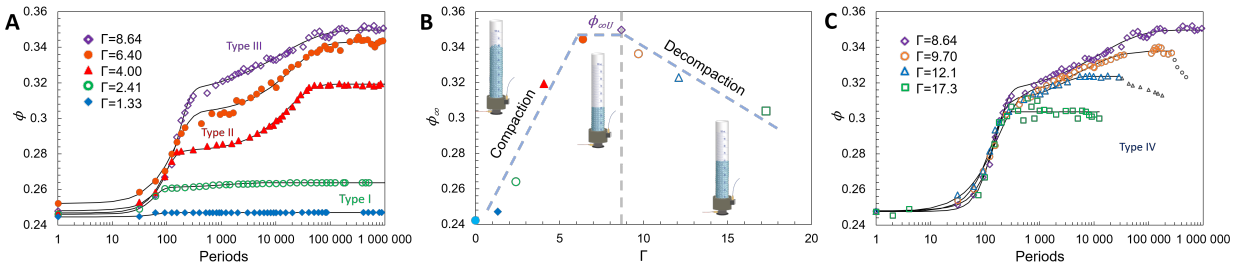

Figure 6: Parametric analysis for the densification of Avicel® PH102, when increasing acceleration with $\Omega = 0.67$ ($f = 30$ Hz). A) Evolution of the packing fraction during compaction; ϕ_∞ increases with Γ. B) ϕ_∞ evolution as a function of Γ. C) Evolution of the packing fraction during decompaction; ϕ_∞ decreases with increasing Γ. For $\Gamma = 17.3$, $\Gamma = 12.1$ and $\Gamma = 9.7$ the granular bed starts to reduce its ϕ after the represented periods (grey marks). Fitted using Eq. 9, generalised KWW model.

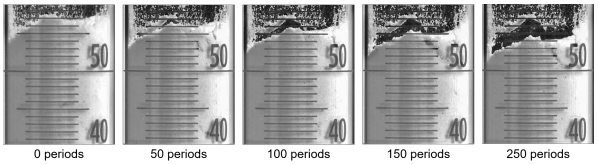

Figure 7: Snapshots of the packing fraction during vibration as a function of the periods N for wheat flour at $\Omega = 1.91$ ($f = 100$ Hz) and $\Gamma = 2.23$ - Type I.

3.4.2. Fluid-like behaviour: two-step compaction.

Once the acceleration is enough to allow particles to jump and separate from one another, the densification kinetics occurs in two steps, during which the medium behaves like a fluid.

In the first compaction step, fluidisation phenomena (bubbling, slugging and turbulent regimes) can be observed during the first periods of vibration. During the second compaction step, the bed densifies while the fluid-like behaviour is reduced to a convective movement.

The fluidisation phenomena observed can be associated with the air trapped within the bulk and the vibration itself since no upward-flowing fluid is injected into the granular bed [17]. Indeed, in our system, the only fluid available is the air trapped within the powder bed. The vibration energy supplied to the powder bed seems to allow the entrainment of the air trapped within the powder bed. The detrainment of the air—the process of bubble escape from the surface—gives rise to surface phenomena depending on the air velocity, in our case to convective movements, granular jets, and even particle entrainment. This fluid-like behaviour of the grains will evolve until it disappears—probably until no more air is available or able to liftoff—the surface bed becomes flat again, and the bulk continues to compact slowly.

Within the fluid-like behaviour, we observed three kinetic behaviours described as follows:

Type II, granular jets. In type II, the volume of the granular bed is slightly reduced and granular jets start to appear; their height increases and then decreases until they disappear. The thickness of the granular jets can be related to the vibration amplitude [8] and described as a function of the pressure of the air trapped within the bulk [46]. Herein, we observed that the granular jets' height and duration were dependent on the nature of the grains and the experimental conditions. For glass beads, the granular jets are thin, high and well dispersed across the sectional area of the container (Fig. 8 upper image); for Avicel® PH102, the jets are nearer to one another, giving a "crown" form, or are adjacent to the walls and shock with it (Fig. 8. lower image); for sericite and wheat flour, the phenomenon could rather be described as an explosion.

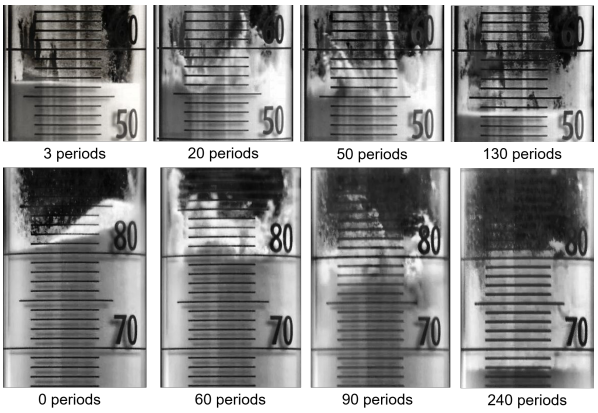

Figure 8: Bulk snapshots at different periods showing granular jets phenomena in type II behaviour. Up - Glass beads, $\Omega = 0.36$ ($f = 30$ Hz) and $\Gamma = 2.4$. Video available as Online resource 4. Down - Avicel® PH102, $\Omega = 0.67$ ($f = 30$ Hz) and $\Gamma = 8.7$.

Concerning the convective movement observed during the second step, Avicel® PH102 shows an

asymmetrical one-sidewall heap (Fig. 9 upper image). Similar behaviour has been observed for glass beads as several authors have noted [7, 9]. For sericite (Fig. 9 lower image), some grains on the surface start to jump and rotate until they form spherical agglomerates that grow with the vibration time even reaching 1 cm as shown in figure 10 (conf. online resource 1). For wheat flour, a similar surface rotation was noted but no real agglomerates were obtained at the end of the experiments. It should be noted that no segregation phenomenon was observed during vibration, even for free-flowing powders.

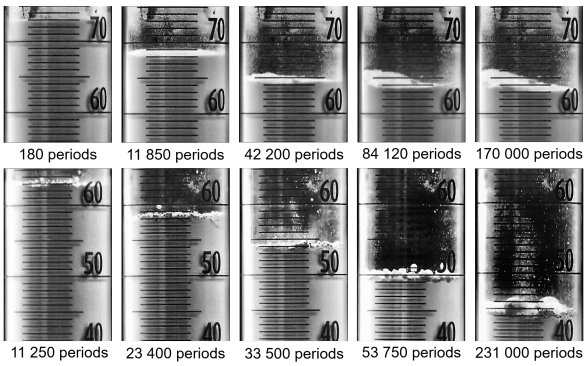

Figure 9: Bulk snapshots at different periods showing the convection movement characteristic of the second compaction step. Up - Avicel®, $\Omega = 0.67$ ($f = 30$ Hz) and $\Gamma = 4.1$. Down - Sericite $\Omega = 0.64$ ($f = 125$ Hz) and $\Gamma = 19.6$. Sericite agglomerates are better illustrated in figure 10.

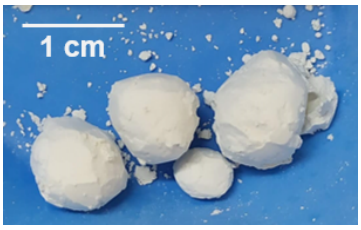

Figure 10: Sericite agglomerates formed during densification by vibration, $\Omega = 0.64$ ($f = 125$ Hz) and $\Gamma = 19.6$. The sizes of the agglomerates range between 0.5 cm and 1 cm.

Type III, bubbling, slugging. Type III results from more intense fluidisation regimes during the first compaction step such as bubbling (Fig. 11 up), slugging (Fig. 11 down) and turbulent (Fig. 12) despite the grains' Geldart classification. It has been shown that vibrated fluidised beds reduce the minimal fluidisation ($v_{mf,v}$) and bubbling velocities allowing type C powders to fluidize [47, 48]. Our experiments seem to corroborate this statement. For C-type powders, sericite and wheat flour, we observed fluidisation phenomena in regimes that were as intense as slugging, round and square nose and right up to turbulent, which is not expected for cohesive powders in classical fluidised beds (see Fig. 12). The bubbling phenomenon is not visible in snapshots of less-cohesive materials such as glass beads and Avicel® PH102 because the grains stick to the vessel walls during fluidisation (see Online resource 2). As expected, increasing the vibration amplitude reduces $v_{mf,v}$ [48] and gives rise to more compacted beds (ϕ_∞).

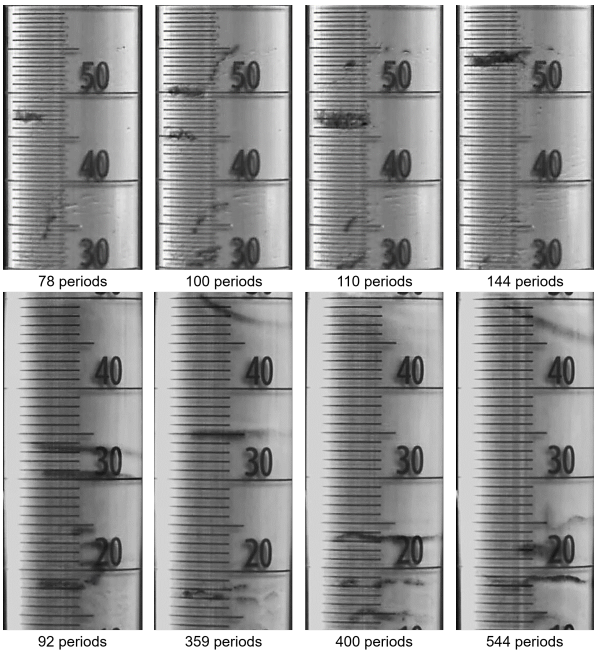

Figure 11: Snapshots showing bubbling and slugging from fluidisation phenomena in type III behaviour. Up -Sericite at $\Gamma = 11.0$ and $\Omega = 0.25$ ($f = 50$ Hz). Down - Wheat flour at $\Gamma = 10.6$ and $\Omega = 0.95$ ($f = 50$ Hz).

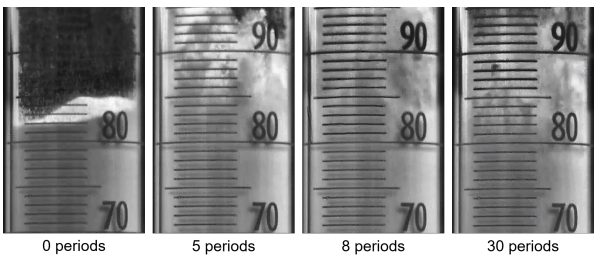

Figure 12: Bulk snapshots at different periods showing powder explosions for Avicel® PH102 at $\Omega = 0.67$ ($f = 30$ Hz) and $\Gamma = 4.99$, type III behaviour.

In type IV, the granular bed decompacts. When the granular bed is submitted to Γ larger than Γ_U, the granular bed decompacts exhibiting a fluid-like

behaviour. From a kinetic perspective, in type IV behaviour, the granular bed densifies until it reaches a stationary state where a convective movement of the grains nearest the surface is observed. In this first compaction state, the higher the Γ, the more the fluidisation phenomena observed is intense (Fig. 14). The densest convective state can be maintained for several periods until, suddenly, the movement of the grains leads to the reincorporation of air into the bulk, allowing the decompaction of the powder bed (Fig. 6.C). The change of behaviour when $\Gamma \geq \Gamma_U$ indicates an energy limit at which some particles can no longer stay together. The energy supplied to the bulk probably allows adhesive interparticle interactions to be overcome which leads or force the grain's mobility and keeps grains from settling or agglomerating (void ratio and coordination number related). The densification kinetics differ for poor and good flowing powders. For good-flowing powders (less cohesive), the densification occurs at the same rate (Fig. 6.C) but the bulk reaches a less compacted state when increasing Γ. However, for poor-flowing powders (more cohesive), the densification rate and the packing fraction do not evolve in the same way as Γ increases (see Fig. 13, $\Gamma = 38.8$). This difference suggests that for more cohesive powders (sericite and wheat flour), the reorganisation at $\Gamma \leq \Gamma_U$ is likely to be affected by clusters (network chain). A further study integrating the densification state through the column to the coordination number could provide a better understanding of this phenomenon and its relation to interparticle forces.

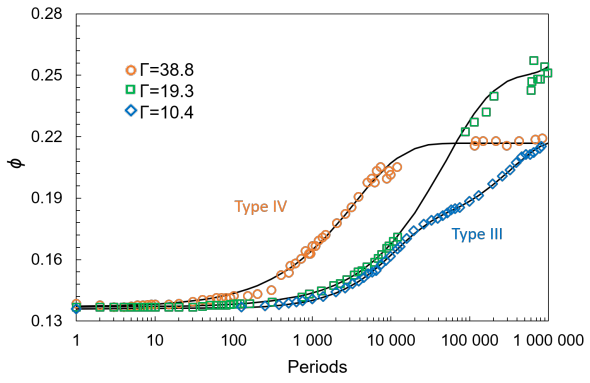

Figure 13: Evolution of the packing fraction of sericite at $\Omega = 0.64$ ($f = 125$ Hz) and different accelerations, indicated in the figure. Fitted using Eq. 9, generalised KWW model.

3.5. The relative frequency, Ω

There are two main observations about the influence of the vibration frequency, Ω, on compaction: 1) the intensity of the fluidisation phenomena observed during vibration reduces when Ω increases. 2) the effect of Ω is related to the flowability of the grains.

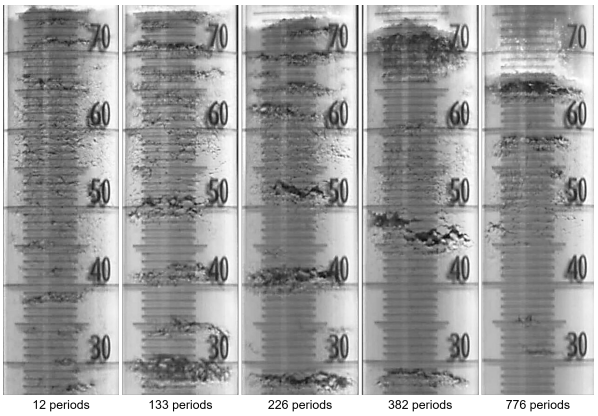

Figure 14: Snapshots showing the slugging from fluidisation phenomena in type IV behaviour for sericite at $\Omega = 0.64$ ($f = 125$ Hz) and $\Gamma = 38.8$.

For poor flowing—more cohesive—samples such as sericite (Fig. 15) and wheat flour (Fig. 17C) at a fixed Γ, increasing Ω gives rise to lower ϕ_∞. Also, the number of periods needed to compact the powder bed increases with Ω as the densification rate ($\Delta\phi/N$) decreases. For example, for sericite, the number of periods needed to reach ϕ_∞ increases with Ω, ranging from $N = 1500$ to $N = 11000$ (see Fig. 15). In terms of model parameters (Eq. 9), the characteristic times τ rises with Ω—for Γ values that allow compaction (see Fig. 6.B). Still, no correlation was found between β and Ω parameters.

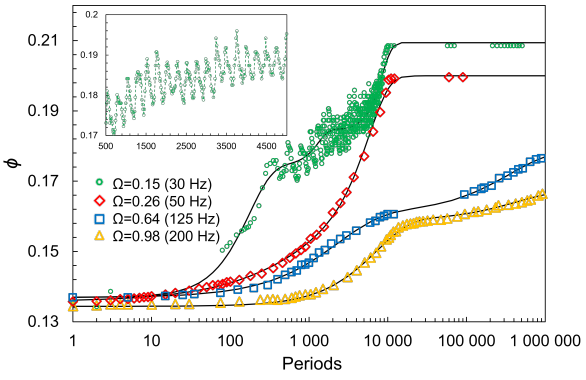

Figure 15: Evolution of the packing fraction of sericite at $\Gamma = 5.0 \pm 0.4$ and different frequencies, indicated in the figure. The inset image depicts in detail the periodic behaviour observed during the second compaction for $\Omega = 0.15$; for clarity, a dashed line connects the experimental points. Fitted using Eq. 9, generalised KWW model.

The increase in Ω reduces the intensity of the

fluidisation phenomena observed, the reorganisation possibilities, and the compaction efficiency, resulting in lower ϕ_∞ values. This might be related to the theoretical meaning of Ω. For cohesionless particles, Ω values smaller than 1 mean that the particles can fall between two periods, which increases reorganisation possibilities. For example, for the same Γ (Fig. 15), we will achieve type III behaviours for the lower frequencies (Ω =0.26 and 0.15) and when Ω increases only type II behaviours will be observed (Ω =0.64 and 0.98). This is coherent with the scientific literature which has reported that increasing the vibration frequency negatively affects vibration-assisted fluidisation [49]. An interesting phenomena was observed for sericite at f = 30 Hz (Fig. 15, Ω=0.15). Initially, the granular bed seems to have reached a convective stationary state but then suddenly, after some periods, the bed increases slightly in height then finally reduces until it reaches a new stationary, more compacted state. The phenomena can be described as if the bulk was breathing in several steps with dilatancy effects (Fig. 16). Dilatancy effects in granular materials have been well reviewed [1, 23, 50]. During dilatancy, the air is inserted into the granular bed to separate the particles enough to avoid interlocking. At oscillation conditions, the compaction is favoured but after a while, the particles' proximity makes it difficult to reorganise, requiring further distance between them to recompact more efficiently. It should be noted that dilatancy phenomena have no analogue in fluids.

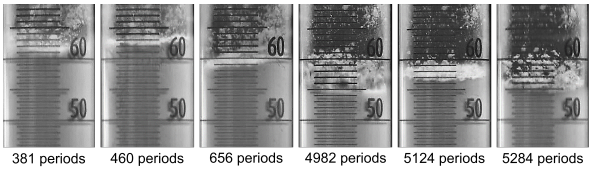

Figure 16: Experimental snapshots of the packing fraction during vibration. Visualisation of oscillatory behaviour for sericite at Γ = 5.2 and Ω = 0.15 (f = 30 Hz).

For wheat flour (Fig. 17C), for low accelerations (Γ= 3.2) and low frequencies (f=30 Hz - Ω =0.57) we observed the type I behaviour (solid-like). When increasing Γ to 16.6, type II and III behaviours can be observed at low frequencies. When Ω increases, the fluidisation phenomena intensity reduces as with sericite and results in a less compacted bed (lower ϕ_∞).

The behaviour of good flowing materials such as glass beads (Fig. 17A) and Avicel® PH102 (Fig. 17B) seems to be less dependent on Ω values. For glass beads, similar Γ values result in similar ϕ_∞ independently of Ω as previously shown in the literature [20]. For Avicel® PH102, experimental results showed small differences at low Γ values.

If the influence of the system geometry is neglected (grains size, vessel, bulk height), the vibration can be described by Γ and Ω. The main parameter that gathers these two dimensionless variables is the vibration energy and for a harmonically driven system–the kinetic energy, $E = mv^2/2$– it can be written as:

$$E_v = \frac{1}{2}m(2\pi f)^2A^2 = \frac{m \cdot a_{p-p}^2}{8(\pi f)^2} = \frac{m}{8}\left(\frac{g\,\Gamma}{\pi\, f}\right)^2 \qquad (10)$$

where m corresponds to the bulk mass and a_{p-p} to the peak-to-peak acceleration [13, 51].

Whether particles reorganize or not depends on the energy supplied to the bulk. It is responsible for the densification of the bulk and the observed phenomena [13, 14, 5]. From Eq. 10, it can be depicted that increasing Γ results in increasing the energy supplied to the powder bed while increasing Ω reduces it, which fits our observations as in the case for the intensification of the phenomena observed. Nonetheless, figure 18 shows that when the E_v is kept constant but Γ and Ω vary, the compaction state of the powder bed changes. This means that the E_v is not the controlling parameter over grains reorganization or densification for complex industrial materials. Previous studies have shown that the reorganization of glass beads (monodisperse between 100 and 1000 μm) under gentle vibration ($\Gamma \leq 3.5$ and $E_v \leq 0.7$ mJ)—without liftoff, in a contact regime—is caused by particle Brownian motion, where the E_v seems to act similarly to the thermal energy on molecular systems near the glass transition, controlling the free volume [51]. Even so, no Brownian motion has been clearly observed for more complex samples, nor for smaller glass beads less than 100 μm (via vibrated rheometer measures [51], not shown herein).

From figure 18, we conclude that to find the densest state (ϕ_U), Γ and Ω parameters should be investigated simultaneously. Lumay et al. [35] suggested that the packing fraction ϕ is an indicator of the cohesiveness of the material, but this is not confirmed by our results (see Fig. 5). Certainly, grains' adhesive interactions (cohesion) play a significant role over powders behaviour but it is a nonexclusive effect over compactness and flowability [42]. The maximal packing fraction and the conditions at which it is obtained (E_v, Γ and Ω) could be described as an intrinsic characteristic of the granular material-geometry system [13]. The energy at which the densest state is obtained represents the equilibrium between different forces acting between particles and

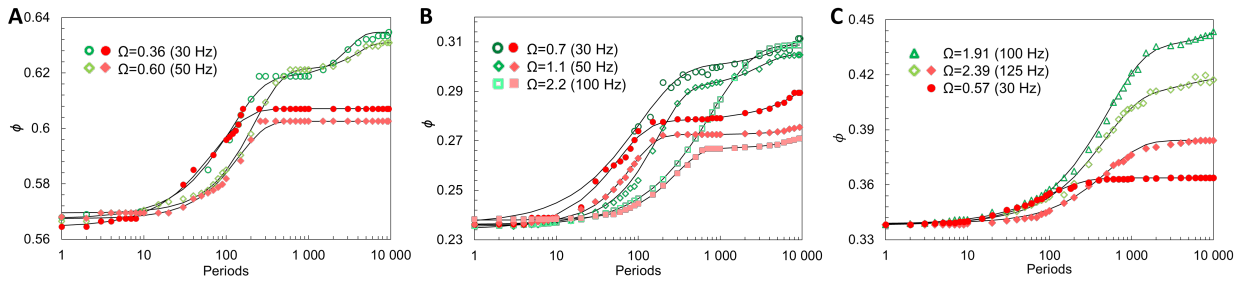

Figure 17: Evolution of the packing fraction for different materials at different frequencies and accelerations. Filled marks indicate the low acceleration and void marks the high acceleration, frequencies are indicated in the figure. A) glass beads: • ♦ $\Gamma = 1.8 \pm 0.1$, ○ ◇ $\Gamma = 3.0 \pm 0.1$. B) Avicel® PH102: • ♦ ■ $\Gamma = 2.63 \pm 0.07$; ○ ◇ □ $\Gamma = 5.5 \pm 0.3$. and C) wheat flour: • ♦ $\Gamma = 3.2 \pm 0.1$; △ ◇ $\Gamma = 16.6 \pm 0.1$. Fitted using Eq. 9, generalised KWW model.

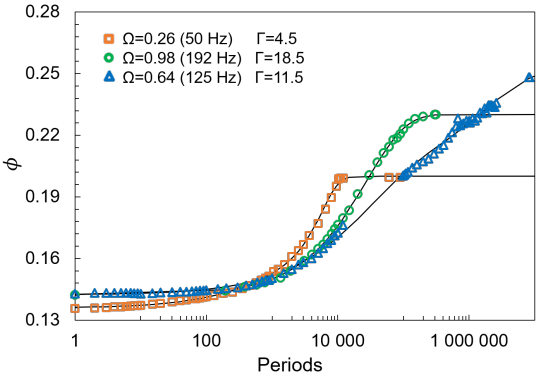

Figure 18: Evolution of the packing fraction of sericite at $E_v = 0.32 \pm 0.02$ mJ, to obtain the same energy frequency and acceleration were varied as indicated in the figure. Fitted using Eq. 9, generalised KWW model.

could represent advantageous knowledge for industrial contexts.

Finally, we have not found the relation between the particle properties (d, ff, c, and ρ_p) and the model parameters (τ and β). Our findings demonstrate a relationship between bulk interparticle forces c and the intensity of the fluidization phenomena observed during densification: less cohesive samples (glass beads and Avicel PH 102) require less energy to fluidize than more cohesive samples (sericite and wheat flour).

The densification kinetics showed larger τ values when Ω increased. Still, the adjustment β parameters do not correlate to any other property or parameter. Interestingly, unlike glass beads, the vibration frequency greatly affected the cohesive samples' packing fraction, i.e., $\phi_\infty = f(\Omega, \Gamma, c)$. This relationship, however, is not linear and is most likely multi-factor dependent. We think particularly of a coupling effect between the strength of interparticle interactions and the ability of the sample to attenuate the vibration (energy dissipation)—not evaluated herein.

4. Conclusions

In this work, we studied the kinetics behaviour of a powder column under vibration. The vibration was harmonically driven using a particle damper and the acceleration, frequency and waiting time between periods were studied in order to evaluate their influence on the dynamics of compaction and the stationary state properties.

We found that for complex granular materials, allowing the media to relax by adding a time between two periods decreases the final packing fraction at similar conditions (Γ and Ω) and also that the bulk densifies, showing a solid-like behaviour when it is allowed to relax. When no relaxation time is allowed, we find a complex time evolution that occurs in multiple steps, generally two, that can be represented as a succession of stretched exponential as in a generalised KWW model.

For good flow materials, small-polydispersed glass beads and Avicel® PH102, the acceleration seems to be responsible for the densification of the bed and thus will define the final packing fraction. At the same time, the frequency will determine the number of periods needed to achieve the steady state. On the contrary, for poorly flowing materials, wheat flour and sericite, both variables— Γ and Ω—will influence the packing fraction while small accelerations and bigger frequencies will give rise to less compacted beds.

We focused on the phenomenology observed during densification. The main difference with classical kinetics studies using non-cohesive, monodispersed, hard spherical particles such as glass beads is that the

granular bed fluidize during the first vibration periods. At fixed frequency, increasing the acceleration was similar to increasing the superficial gas velocity giving rise to different flow regimes going from bubbling to slugging to turbulent. Interestingly, our system seems to work similarly to vibratory fluidised beds because group C powders, such as wheat flour and sericite, were fluidised, showing bubbling and even flat slugging regimes which is not generally expected for cohesive powders in classical fluidised beds.

Finally, the kinetics curve shape was associated with a specific fluidisation phenomenon. For type I kinetics, the compaction process occurs in a single step and the powder bed behaves as a solid. In Type II, densification occurs in two-compaction stages that are well separated from each other. Here the fluid-like behaviour is reduced to granular jets. In type III, the two-compaction steps are not that clearly separated and the fluidisation is more intense which involves bubbling, slugging and powder explosions. In Type IV kinetics, the energy supplied to the system prevents particles from settling and the powder bed decompacts. The kinetic behaviour seems similar to type III but the phenomena are more intense in these. After reaching a convective temporary stationary state, the powder bed begins to aerate, resulting in less compacted beds.

All the videos from the snapshots presented in the article are available openly in the DOREL repository from the Université de Lorraine https://doi.org/10.12763/OHJ5CH.

Online resource 1. Video of the granulation observed for sericite at $\Gamma = 11.5$ and $\Omega = 0.64$ ($f = 125$ Hz), at the end of the experiment. Online resource 2. Video of the bubbling observed for Avicel® PH102 at $\Gamma = 5.34$ and $\Omega = 0.67$ ($f = 30$ Hz).

References

[1] H. M. Jaeger, J. B. Knight, C. H. Liu, S. Sidney, R. Nagel, What Is Shaking in the Sandbox?, MRS Bulletin 19 (5) (1994) 25–31. doi:10.1557/S0883769400036538.

[2] M. G. Cares-Pacheco, V. Falk, A phenomenological law for complex granular materials from mohr-coulomb theory, Advanced Powder Technology 34 (1) (2023) 103888. doi:10.1016/j.apt.2022.103888.

[3] R. Linemann, J. Runge, M. Sommerfeld, U. Weißgüttel, Compaction of Powders due to Vibrations and Shocks, Particle and Particle Systems Characterization 21 (4) (2004) 261–267. doi:10.1002/ppsc.200400938.

[4] S. Klongboonjit, S. Campbell, Convection in deep vertically shaken particle beds. I. General features, Physics of Fluids 20 (10) (2008). doi:10.1063/1.2996134.

[5] F. Ludewig, S. Dorbolo, T. Gilet, N. Vandewalle, Energetic approach for the characterization of taps in granular compaction, Epl 84 (4) (2008). doi:10.1209/0295-5075/84/44001.

[6] A. W. Roberts, Vibration of Fine Powders and Its application, in: Handbook of Powder Science and Technology, Chapman and Hall, New York, 1997, Ch. 5, pp. 146–201.

[7] E. Clément, L. Labous, L. Vanel, Granular Packing Under Vibration, Europhysics news 29 (3) (1998) 107. doi:10.1007/s007700050069.

[8] P. Evesque, Shaking dry powders and grains, Contemporary Physics 33 (4) (1992) 245–261. doi:10.1080/00107519208223973.

[9] P. Philippe, D. Bideau, Granular Medium under Vertical Tapping: Change of Compaction and Convection Dynamics around the Liftoff Threshold, Physical Review Letters 91 (10) (2003) 1043021–1043024. doi:10.1103/PhysRevLett.91.104302.

[10] G. V. Barbosa-Cánovas, P. Juliano, Compression and compaction characteristics of selected food powders, in: Advances in Food and Nutrition Research, vol.: 49 Edition, Elsevier Inc., 2005, pp. 233–307.

[11] M. Masmoudi, S. Job, M. S. Abbes, I. Tawfiq, M. Haddar, Experimental and numerical investigations of dissipation mechanisms in particle dampers, Granular Matter 18 (3) (2016) 1–11. doi:10.1007/s10035-016-0667-4.

[12] H. H. Hausner, Friction conditions in a mass of metal powder, International Journal of Powder Methallurgy 3 (4) (1967) 7–13.

[13] A. Saker, M.-G. Cares-Pacheco, P. Marchal, V. Falk, Powders flowability assessment in granular compaction: What about the consistency of Hausner ratio?, Powder Technology 354 (2019) 52–63. doi:10.1016/j.powtec.2019.05.032.

[14] M.-G. Cares Pacheco, M.-C. Jiménez Garavito, A. Ober, F. Gerardin, E. Silvente, V. Falk, Effects of humidity and glidants on the flowability of pharmaceutical excipients. An experimental energetical approach during granular compaction, International Journal of Pharmaceutics 604 (May) (2021) 120747. doi:10.1016/j.ijpharm.2021.120747.

[15] R. L. Carr, Evaluating flow properties of solids, Chemical Engineering 72 (69) (1965) 163–168.

[16] T. Boutreux, P. G. D. Gennes, Compaction of granular mixtures: A free volume model, Physica A: Statistical Mechanics and its Applications 244 (1997). doi:10.1016/S0378-4371(97)00236-7.

[17] B. Andreotti, Y. Forterre, O. Pouliquen, Les millieux granulaires entre fluide et solide, EDP Sciences, Courtaboeuf, 2011.

[18] E. Rondet, M. Delalonde, S. Chuetor, T. Ruiz, Modeling of granular material's packing: Equivalence between vibrated solicitations and consolidation, Powder Technology 310 (2017) 287–294. doi:10.1016/j.powtec.2016.12.056.

[19] H. O. N. Altino, G. A. Lourenço, C. H. Ataíde, System development for bulk density data acquisition of granular materials: Effect of operational conditions and optimization, Powder Technology 391 (2021) 184–197. doi:10.1016/j.powtec.2021.06.013.

[20] P. Ribière, P. Richard, P. Philippe, D. Bideau, R. Delannay, On the existence of stationary states during granular compaction, European Physical Journal E 22 (3) (2007) 249–253. doi:10.1140/epje/e2007-00017-x.

[21] United States Pharmacopeial Convention, Bulk density and tapped density of powders (2015).

[22] J. B. Knight, C. G. Fandrich, C. N. Lau, H. M. Jaeger, S. R. Nagel, Density relaxation in a vibrated granular material, Physical Review E 51 (5) (1995) 3957–3963. doi:10.1103/PhysRevE.51.3957.

[23] H. M. Jaeger, S. R. Nagel, R. P. Behringer, Granular solids, liquids, and gases, Reviews of Modern Physics 68 (4) (1996) 1259–1273. doi:10.1103/RevModPhys.68.1259.

[24] J. Malave, G. V. Barbosa-Canovas, M. Peleg, Comparison of the Compaction Characterisitics of Selected Food Powders by Vibration, Tapping and Mechanical Compression, Journal of Food Science 50 (5) (1985) 1473–1476. doi:10.1111/j.1365-2621.1985.tb10502.x.

[25] T. Akiyama, Y. Miyamoto, N. Yamanaka, J. Q. Zhang, Densification of powders by means of air, vibratory and mechanical compactions, Powder Technology 46 (2-3) (1986) 173–180. doi:10.1016/0032-5910(86)80024-9.

[26] A. B. Yu, J. S. Hall, Packing of fine powders subjected to tapping, Powder Technology 78 (3) (1994) 247–256. doi:10.1016/0032-5910(93)02790-H.

[27] C. Josserand, A. V. Tkachenko, D. M. Mueth, H. M. Jaeger, Memory effects in granular materials, Physical Review Letters 85 (17) (2000) 3632–3635. arXiv:0002401, doi:10.1103/PhysRevLett.85.3632.

[28] G. Lumay, N. Vandewalle, Experimental study of granular compaction dynamics at different scales: Grain mobility, hexagonal domains, and packing fraction, Physical Review Letters 95 (2) (2005) 8–11. doi:10.1103/PhysRevLett.95.028002.

[29] J. C. Quezada, G. Saussine, P. Breul, F. Radjaï, Predicting the settlement of coarse granular materials under vertical loading, Scientific Reports 4 (2014) 2–6. doi:10.1038/srep05707.

[30] S. Kiesgen de Richter, C. Hanotin, P. Marchal, S. Leclerc, F. Demeurie, N. Louvet, Vibration-induced compaction of granular suspensions, European Physical Journal E 38 (7) (2015). doi:10.1140/epje/i2015-15074-7.

[31] J. E. Mathonnet, P. Sornay, M. Nicolas, B. Dalloz-Dubrujeaud, Compaction of noncohesive and cohesive granular materials under vibrations: Experiments and stochastic model, Physical Review E 95 (4) (2017) 1–6. doi:10.1103/PhysRevE.95.042904.

[32] K. Kawakita, K. H. Lüdde, Some considerations on powder compression equations, Powder Technology 4 (2) (1971) 61–68. doi:10.1016/0032-5910(71)80001-3.

[33] T. Sone, Consistency of Foodstuffs, Springer Netherlands, Dordrecht, 1972. doi:10.1007/978-94-010-2876-9.

[34] R. W. Heckel, Density-pressure relationships in powder compaction, Transactions of the Metallurgical Society of AIME 221 (1961).

[35] G. Lumay, N. Vandewalle, C. Bodson, L. Delattre, O. Gerasimov, Linking compaction dynamics to the flow properties of powders, Applied Physics Letters 89 (9) (2006) 1–4. doi:10.1063/1.2338801.

[36] E. Nowak, J. Knight, E. Ben-Naim, H. Jaeger, S. Nagel, Density fluctuations in vibrated granular materials, Physical Review E 57 (2) (1998) 1971–1982. doi:10.1103/PhysRevE.57.1971.

[37] P. Ribière, P. Richard, R. Delannay, D. Bideau, Importance of convection in the compaction mechanisms of anisotropic granular media, Physical Review E 71 (1) (2005) 011304. doi:10.1103/PhysRevE.71.011304.

[38] P. Richard, M. Nicodemi, R. Delannay, P. Ribière, D. Bideau, Slow relaxation and compaction of granular systems (2005). doi:10.1038/nmat1300.

[39] P. Philippe, D. Bideau, Numerical model for granular compaction under vertical tapping, Physical Review E 63 (5) (2001) 051304. doi:10.1103/PhysRevE.63.051304.

[40] E. Caglioti, V. Loreto, H. J. Herrmann, M. Nicodemi, A "tetris-like" model for the compaction of dry granular media, Physical Review Letters 79 (1997). doi:10.1103/PhysRevLett.79.1575.

[41] J. Talbot, G. Tarjus, P. R. V. Tassel, P. Viot, From car parking to protein adsorption: An overview of sequential adsorption processes, Colloids and Surfaces A: Physicochemical and Engineering Aspects 165 (2000). doi:10.1016/S0927-7757(99)00409-4.

[42] M.-C. Jiménez Garavito, M.-G. Cares-Pacheco, F. Gerardin, V. Falk, Silica nanoparticles as glidants for industrial processing: why, how and how much?, Industrial & Engineering Chemistry Research (2022).

[43] J. R. Grace, Contacting modes and behaviour classification of gas-solid and other two-phase suspensions, The Canadian Journal of Chemical Engineering 64 (3) (1986) 353–363. doi:10.1002/cjce.5450640301.

[44] T. Akiyama, K. M. Aoki, K. Yamamoto, T. Yoshikawa, Experimental study on vibration-induced convection and heaping in granular beds, Granular Matter 1 (1) (1998) 15–20. doi:10.1007/pl00010905.

[45] G. C. Barker, A. Mehta, Transient phenomena, self-diffusion, and orientational effects in vibrated powders, Physical Review E 47 (1) (1993) 184–188. doi:10.1103/PhysRevE.47.184.

[46] J. R. Royer, E. I. Corwin, A. Flior, M. L. Cordero, M. L. Rivers, P. J. Eng, H. M. Jaeger, Formation of granular jets observed by high-speed X-ray radiography, Nature Physics 1 (3) (2005) 164–167. doi:10.1038/nphys175.

[47] Y. Mawatari, Y. Tatemoto, K. Noda, Prediction of minimum fluidization velocity for vibrated fluidized bed, Powder Technology 131 (1) (2003) 66–70. doi:10.1016/S0032-5910(02)00323-6.

[48] W. Brennan, M. Jacobson, G. Book, C. Briens, L. Briens, Development of a tribolelectric procedure for the measurement of mixing and drying in a vibrated fluidized bed, Powder Technology 181 (2) (2008) 178–185. doi:10.1016/j.powtec.2006.12.002.

[49] D. Barletta, G. Donsì, G. Ferrari, M. Poletto, P. Russo, The effect of vibrations on fluidized cohesive powders, in: The 12th International Conference on Fluidization- New Horizons in Fluidization Engineering, 2007, pp. 377–384.

[50] B. Thomas, M. O. Mason, A. M. Squires, Some behaviors of shallow vibrated beds across a wide range in particle size and their implications for powder classification, Powder Technology 111 (1-2) (2000) 34–49. doi:10.1016/S0032-5910(00)00237-0.

[51] P. Marchal, N. Smirani, L. Choplin, Rheology of dense-phase vibrated powders and molecular analogies, Journal of Rheology 53 (2009). doi:10.1122/1.3037266.